

smallest size  $r$ . It is formed by a gradual deformation of an  $\eta$ -size region with an initially uniform concentration. The shock contribution to the moment,  $\langle \bar{n}^2[r] \rangle \propto \int dx (\partial \bar{n} / \partial x)^2 \propto \ln(l/r)^{1/2}$ , contains a logarithm that is of order unity in our case. Therefore, we neglect shocks and consider fluctuations with  $|\sigma| < \tau^{-1}$ . The smallest size of the region evolves as  $\eta \exp[\lambda_d t]$ , where  $\lambda_d$  is the most negative Lyapunov exponent estimated as  $|\lambda_d| \approx \int dt \langle \text{tr}(\sigma^T(0)\sigma(t)) \rangle = \lambda \bar{c} = \lambda \epsilon (1 + \epsilon^2)^{-1/2}$ . Therefore, concentration fluctuations accumulate during the time  $\ln(\eta/r)/|\lambda_d|$ . Because  $\dot{n} = -n\tau\sigma$  in the droplets' frame and the contribution of each cluster to the spatial average is proportional to its volume  $\exp[\int_0^t \text{tr}(\sigma^T(t')\sigma(t')) dt']$ , we obtain:

$$\begin{aligned} \langle \bar{n}^2[r] \rangle &= \langle n \rangle^2 \left\langle \exp \left[ - \int_0^{\ln(\eta/r)/\lambda_d} \text{tr}(\sigma^T(t')\sigma(t')) dt' \right] \right\rangle \\ &= \langle n \rangle^2 \left\langle \exp \left[ \tau \int_0^{\ln(\eta/r)/\lambda_d} \text{tr}(\sigma^2(t')) dt' \right] \right\rangle = \langle n \rangle^2 \left( \frac{\eta}{r} \right)^\alpha, \text{ for } \alpha \\ &= \tau^2 / |\lambda_d| \int dt \langle \text{tr}(\sigma^T(0)\sigma(t)) \rangle \end{aligned} \quad (5)$$

where we assumed that  $\ln(\eta/r)/|\lambda_d|$  is much larger than the correlation time of  $\text{tr}\sigma^2$ . The higher terms of the cumulant expansion cannot be parametrically larger than the estimate (5) since they contain integrals estimated as  $\langle \text{tr}\sigma^2 [\tau \tau_c(\sigma) \text{tr}\sigma^2]^{2m+1} \rangle$ , for  $m \geq 1$ , and both the correlation time  $\tau_c(\sigma)$  and  $\tau$  are less than  $|\sigma|^{-1}$  in the integration domain. Moreover, if  $\langle \tau^2 \tau_c(\sigma) (\text{tr}\sigma^2)^2 \rangle$  is determined by  $|\sigma| \ll \tau^{-1}$  then equation (5) is correct not only parametrically but also numerically. To evaluate  $\alpha$  we express it via the single-time PDF  $P(|\sigma|)$ :

$$\alpha = (\tau^2 / \lambda \epsilon) \int_{|\sigma| < \tau^{-1}} d\sigma \sigma^4 \tau_c(\sigma) P(|\sigma|) \quad (6)$$

To relate  $P(\sigma)$  to  $\mathcal{P}(s)$  measured experimentally we note that  $\tau_c(s) > \tau$  for  $s < s^* = \tau^{-1} \min\{1, \epsilon^2/St\}$  so that  $P(|\sigma|) = P(|s| = |\sigma|)$  there. At  $s > s^*$  the fluctuations of  $s$  contributing to  $P(\sigma)$  have  $\tau_c(s) < \tau$  and can occur at any moment within  $\tau$ . The extrapolation formulas at  $St < \epsilon$  are  $P(|\sigma|) = (1 + \sigma^2/s_*^2) \mathcal{P}(|s| = |\sigma| + \sigma^2/s_*)$  and  $\tau_c(|\sigma|) = \tau + (|\sigma| + \lambda^{1/2} |\sigma|^{1/2} \epsilon^{-1})^{-1}$ . Our theory is valid as long as  $St \text{min}\{1, \epsilon\} < 1$ .

Received 28 February; accepted 11 July 2002; doi:10.1038/nature00983.

1. Pruppacher, H. & Klett, J. *Microphysics of Clouds and Precipitation* (Kluwer, Dordrecht, 1998).
2. Seinfeld, J. & Pandis, S. *Atmospheric Chemistry and Physics* (Wiley, New York, 1998).
3. Pinsky, M., Khain, A. & Shapiro, M. Stochastic effects of cloud droplet hydrodynamic interaction in a turbulent flow. *Atmos. Res.* **53**, 131–169 (2000).
4. Jonas, P. Turbulence and cloud microphysics. *Atmos. Res.* **40**, 283–306 (1996).
5. Vaillancourt, P. A. & Yau, M. K. Review of particle-turbulence interactions and consequences for cloud physics. *Bull. Am. Met. Soc.* **81**, 285–298 (2000).
6. Maxey, M. R. The gravitational settling of aerosol particles in homogeneous turbulence and random flow field. *J. Fluid Mech.* **174**, 441–465 (1987).
7. Squires, K. & Eaton, J. Measurements of particle dispersion from direct numerical simulations of isotropic turbulence. *J. Fluid Mech.* **226**, 1–35 (1991).
8. Pinsky, M. & Khain, A. Turbulence effects on droplet growth and size distribution in clouds—a review. *J. Aerosol Sci.* **28**, 1177–1214 (1997).
9. Sundaram, S. & Collins, L. Collision statistics in an isotropic particle-laden turbulent suspension. *J. Fluid Mech.* **335**, 75–109 (1997).
10. Zhou, Y., Wexler, A. & Wang, L.-P. Modelling turbulent collision of bidisperse inertial particles. *J. Fluid Mech.* **433**, 77–104 (2001).
11. Reade, W. & Collins, L. Effect of preferential concentration on turbulent collision rates. *Phys. Fluids* **12**, 2530–2540 (2000).
12. Wang, L. P. & Maxey, M. Settling velocity and concentration distribution of heavy particles in homogeneous isotropic turbulence. *J. Fluid Mech.* **256**, 27–68 (1993).
13. Balkovsky, E., Falkovich, G. & Fouxon, A. Intermittent distribution of inertial particles in turbulent flows. *Phys. Rev. Lett.* **86**, 2790–2793 (2001).
14. Brumfiel, G. How raindrops form. *Phys. Rev. Focus* **7**, story 14 (22 March 2001), <http://focus.aps.org/v7/st14.html>.
15. Shraiman, B. & Siggia, E. Scalar turbulence. *Nature* **405**, 639–646 (2000).
16. Falkovich, G., Gawedzki, K. & Vergassola, M. Particles and fields in fluid turbulence. *Rev. Mod. Phys.* **73**, 913–975 (2001).
17. Pinsky, M., Khain, A. & Shapiro, M. Collision efficiency of drops in a wide range of Reynolds numbers. *J. Atmos. Sci.* **58**, 742–766 (2001).
18. Johnson, D. B. The role of giant and ultragiant aerosol particles in warm rain initiation. *J. Atmos. Sci.* **39**, 448–460 (1982).
19. Levin, Z., Wurzler, S. & Reisin, T. Modification of mineral dust particles by cloud processing and subsequent effects on drop size distribution. *J. Geophys. Res.* **105**, 4501–4512 (2000).
20. Saffman, P. & Turner, J. On the collision of drops in turbulent clouds. *J. Fluid Mech.* **1**, 16–30 (1956).
21. Raju, N. & Meiburg, N. The accumulation and dispersion of heavy particles in forced two-dimensional mixing layers. *Phys. Fluids* **7**, 1241–1264 (1995).
22. Maxey, M. R. & Riley, J. J. Equation of motion for a small rigid sphere in a nonuniform flow. *Phys. Fluids* **26**, 883–889 (1983).
23. Vekstein, G. *Physics of Continuous Media: A Collection of Problems with Solutions* 93–94 (Adam Hilger, Bristol, 1992).
24. Grits, B., Pinsky, M. & Khain, A. Formation of small-scale droplet concentration inhomogeneity in a turbulent flow as seen from experiments with an isotropic turbulence model. *Proc. 13th Int. Conf. on Clouds and Precipitation* Vol. 1, 138–141 (Am. Met. Soc., Reno, 2000).
25. Kostinski, A. & Shaw, R. Scale-dependent droplet clustering in turbulent clouds. *J. Fluid Mech.* **434**, 389–398 (2001).
26. Brenguier, J.-L. & Chumat, L. Droplet spectra broadening in cumulus clouds. *J. Atmos. Sci.* **58**, 628–641 (1999).

27. Belin, F., Maurer, J., Tabeling, P. & Willaime, H. Velocity gradient distribution in fully developed turbulence: an experimental study. *Phys. Fluids* **9**, 3843–3850 (1997).
28. Davila, J. & Hunt, J. C. R. Settling of small particles near vortices and in turbulence. *J. Fluid Mech.* **440**, 117–145 (2001).
29. Crowe, C. T., Chung, J. N. & Troutt, T. R. *Particulate Two Phase Flow* Ch. 18 (ed. Roce, M. C.) 626 (Butterworth-Heinemann, Oxford, 1993).
30. Marble, F. E. Dynamics of dusty gases. *Annu. Rev. Fluid Mech.* **2**, 397–461 (1970).

**Acknowledgements**

We thank A. Khain, V. Lebedev and M. Pinsky for discussions, and the Minerva and Israel Science Foundations for support.

**Competing interests statement**

The authors declare that they have no competing financial interests.

Correspondence and requests for materials should be addressed to G.F. (e-mail: finfal@wicc.weizmann.ac.il).

**Macroecological patterns of phytoplankton in the northwestern North Atlantic Ocean**

W. K. W. Li

*Biological Oceanography Section, Bedford Institute of Oceanography, Department of Fisheries and Oceans, Dartmouth, Nova Scotia B2Y 4A2, Canada*

Many issues in biological oceanography are regional or global in scope<sup>1</sup>; however, there are not many data sets of extensive areal coverage for marine plankton. In microbial ecology, a fruitful approach to large-scale questions is comparative analysis<sup>2,3</sup> wherein statistical data patterns are sought from different ecosystems, frequently assembled from unrelated studies<sup>4</sup>. A more recent approach termed macroecology characterizes phenomena emerging from large numbers of biological units by emphasizing the shapes and boundaries of statistical distributions, because these reflect the constraints on variation<sup>5</sup>. Here, I use a set of flow cytometric measurements to provide macroecological perspectives on North Atlantic phytoplankton communities. Distinct trends of abundance in picophytoplankton and both small and large nanophytoplankton underlaid two patterns. First, total abundance of the three groups was related to assemblage mean-cell size according to the 3/4 power law of allometric scaling in biology<sup>6,7</sup>. Second, cytometric diversity<sup>8</sup> (an ataxonomic measure of assemblage entropy) was maximal at intermediate levels of water column stratification<sup>9</sup>. Here, intermediate disturbance shapes diversity through an equitable distribution of cells in size classes, from which arises a high overall biomass. By subsampling local fluctuations, macroecology reveals meaningful patterns of phytoplankton at large scales.

The data were collected from 23 oceanographic cruises spanning a 13-year period. We have published previously a description of the 14 earlier cruises (1989–98), a map of the stations, and sampling methods<sup>10</sup>. More recently (1999–2001), we re-occupied the stations on the Scotian shelf in spring and autumn, and the Labrador Sea in spring. Although stations were located across seven biogeochemical provinces<sup>1</sup>, only measurements in the four northwestern ones, representing 82% of the data set, were included in the present analysis. These four contiguous provinces were Atlantic Arctic (ARCT), boreal polar (BPLR), northwest Atlantic shelves (NWCS) and Gulf Stream (GFST). The stations were in an area bounded approximately by 38° N, 61° N, 42° W and 67° W. The extracted data

set comprised 6,339 seawater samples collected from an average of 9 to 10 depths in the photic zone of 656 hydrocasts. Although large, this data set lacked any winter measurements.

These data sets provide a clear delineation of phytoplankton variability in the ocean afforded by thousands of measurements. In a plot of phytoplankton abundance against chlorophyll biomass, the boundaries and internal structure of the data domain are indicated by colour-coded density regions (Fig. 1a). A polygon to encompass the data is given by the unit contour line, which excludes apparent outliers. This polygon has two rising edges: the bottom edge was defined by spring phytoplankters, whereas the top edge was defined by autumn phytoplankters. Large cells were more prevalent in spring whereas small cells were more so in autumn. The polygon also has a falling top edge such that above approximately 0.5 mg chlorophyll per m<sup>3</sup>, maximum cell abundance decreased with increasing biomass, indicating the importance of large cells. This transition level of biomass may be the maximum potential for the picoplankton (<2 μm) component of the community<sup>11</sup>. At higher levels of photoautotrophic biomass, a substantial contribution is expected from the microphytoplankton, which were not counted. However, the upper boundary of the polygon would be largely unaltered because microphytoplankton in these waters, mainly diatoms and dinoflagellates, occur at concentrations between 1 and 1,000 cells ml<sup>-1</sup>, which are too low to make a significant difference.

The structure of flow cytometric signatures for individual samples can be expressed by an index of so-called cytometric

diversity<sup>8</sup>. In this approach, the classification of phytoplankton is based not on taxonomy, but on ataxonomic categories in the bivariate biooptical domain of cell size and chlorophyll content defined by flow cytometric light scatter and red fluorescence. As such, cytometric diversity indicates richness in physiological as well as genetic variations. The index of cytometric diversity is calculated as Hill's diversity number of order one<sup>12</sup>; in other words, it is the exponential Shannon–Wiener index of the cytometric categories (exp  $H'$ ). It is a measurement embodying the ideas of richness and evenness that define the uncertainty of an organism sampled at random<sup>13</sup>; it is also a measurement of widespread use in phytoplankton ecology<sup>9</sup>.

In the northwestern North Atlantic, the scatter plot of cytometric diversity against phytoplankton abundance filled a triangular polygon (Fig. 1b), indicating maximum diversity at an intermediate abundance of about 2,000 cells ml<sup>-1</sup>. Phenomenologically, maximum diversity was a balance between richness and evenness. As more cells appeared in the community, diversity increased because new categories were added. However, as even more cells appeared, they were added to existing categories giving them dominant status, thus decreasing evenness and diversity.

A striking pattern was revealed in the manner in which different size classes were related to the total standing stock of chlorophyll *a* biomass (Fig. 2a). In the range of chlorophyll from about 10 to

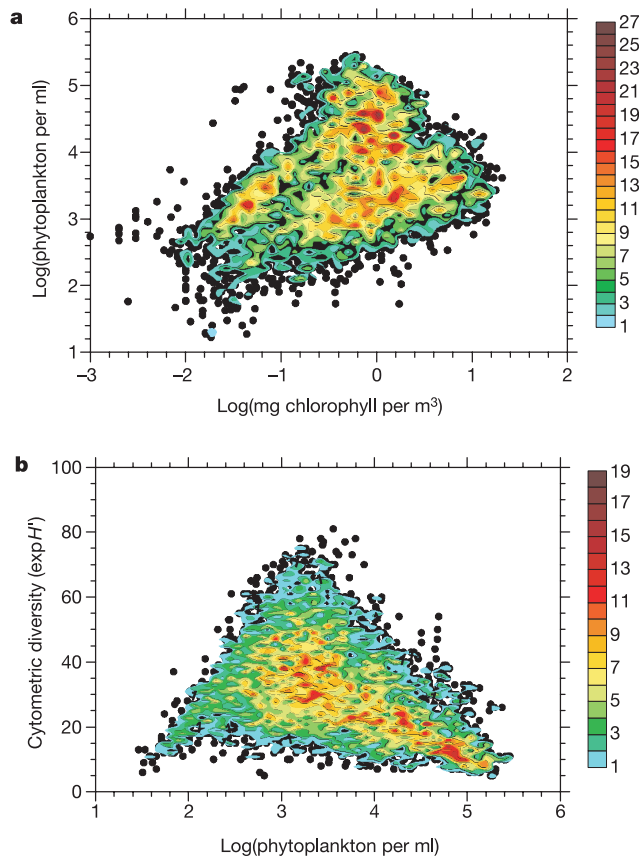


**Figure 1** Range of phytoplankton variability in the northwestern North Atlantic Ocean. **a**, Phytoplankton abundance versus chlorophyll concentration on a volumetric basis. **b**, Cytometric diversity<sup>8</sup> versus phytoplankton abundance. Samples were collected by Niskin bottles from depths of 0–100 m. The geographic distribution of the samples ( $n = 6,339$ ) was 10% ARCT, 11% BPLR, 14% GFST and 65% NWCS. Contour levels indicate the number of overlapping data points in a grid region; the colour code indicates density.  $H'$ , Shannon–Wiener index.

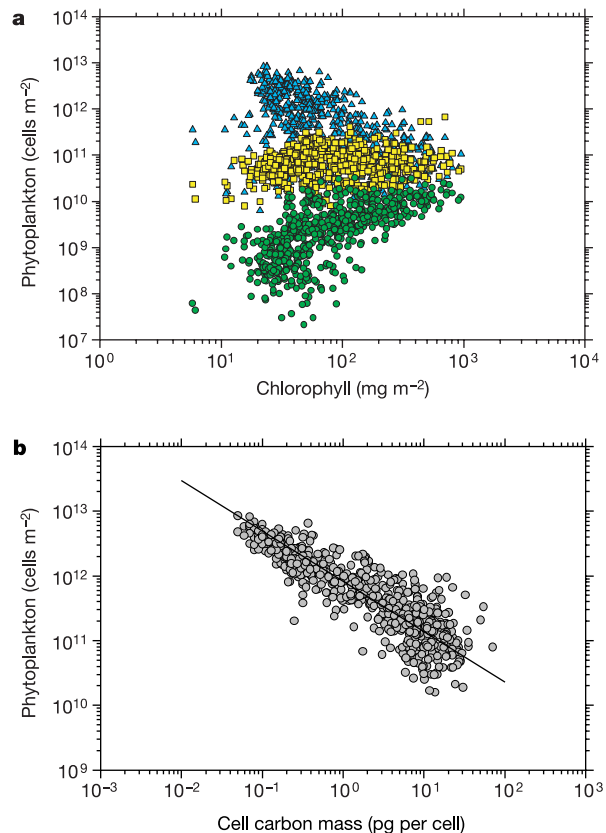


**Figure 2** Relationship of phytoplankton abundance to biomass and mean cell mass. **a**, Phytoplankton abundance versus chlorophyll concentration on an areal basis ( $n = 656$ ). Picophytoplankton (<2 μm, blue triangles), small nanophytoplankton (2–10 μm, yellow squares) and large nanophytoplankton (10–20 μm, green circles) were classified by reference to forward light scatter. Areal values were calculated by trapezoidal integration of volumetric values from 0 to 100 m. **b**, Phytoplankton abundance on an areal basis versus cellular carbon mass. Cell carbon was calculated from cell volume<sup>19</sup>, which was based on the mean equivalent spherical diameter of the phytoplankton assemblage. The assemblage was an abundance-weighted average from 0 to 100 m depth. The line is the model II regression  $\log N = 11.91 - 0.78 \log M_C$ .

1,000 mg m<sup>-2</sup>, a decrease in picoplankton (<2 μm) was mirrored by an increase in large nanoplankton (10–20 μm); however, small nanoplankton (2–10 μm) remained relatively invariant throughout. Here, the picoplankton were primarily *Synechococcus* cyanobacteria and small eukaryotic algae. There were no indications of *Prochlorococcus* cyanobacteria on the Scotian shelf or the Labrador Sea. The small nanoplankton were rich in 19'-hexanoyloxyfucoxanthin, indicating prymnesiophytes. The large nanoplankton were rich in fucoxanthin, indicating primarily diatoms but including other algae as well (Bouman *et al.*, manuscript in preparation). It is widely held that marine phytoplankton communities are assembled by adding larger cells to a relatively uniform background of smaller cells<sup>11,14,15</sup>. The results here indicate that this uniform background is in fact the small nanoplankton. As phytoplankton communities grade from low to high biomass, there is a reduction in picoplankton, an increment in large nanoplankton, and no apparent net change in small nanoplankton.

These systematic patterns in the different size groups lead to phytoplankton communities that conform to an apparently universal relationship between population density and organism size<sup>16</sup>. The principles of allometric scaling<sup>6,7</sup> proceed from a large body of observations that relate metabolic rate (*B*) to body mass (*M*) according to the 3/4 power law,  $B = B_0 M^{3/4}$ , where *B*<sub>0</sub> is a proportionality coefficient. From this, the allometric basis for population density of terrestrial plants can be interpreted as follows<sup>17</sup>. In individual plants, the rate of resource use (*Q*) is proportional to *B*, and thus  $Q \propto M^{3/4}$ . The number of individuals per unit area (*N*) that can be supported by a rate of resource supply (*R*) is  $N = RQ^{-1}$ .

It then follows that  $N \propto M^{-3/4}$ . Geometric mean model II regression<sup>18</sup> of the North Atlantic phytoplankton data (Fig. 2b) indicates that  $\log N = 11.91 - 0.78 \log M_C$ , where *M*<sub>C</sub> is the carbon mass per cell calculated from the mean equivalent spherical diameter of the phytoplankton assemblage using an allometric formula to convert cell volume to cell carbon<sup>19</sup>. The slope is indistinguishable from -0.75 ( $r^2 = 0.77$ ,  $n = 635$ , 95% confidence interval = -0.74 to -0.81). This result greatly extends the generality of the 3/4 power law for phytoplankton beyond laboratory cultures of freshwater chlorophytes<sup>20</sup> and marine species in a coastal fjord of Sweden<sup>21</sup>.

In the ocean, phytoplankton community structure is shaped heavily by physical processes of advection and turbulence<sup>22</sup>. Recent work<sup>23</sup> points to the direct influence of mesoscale vertical motion on the slope of the phytoplankton size–abundance spectrum: upward motion retains large cells in the upper layer against their sinking tendency and therefore results in a flatter spectrum slope. In the limit of maximum upward water motion, the least negative slopes were about -0.75, in accord with the general law. By contrast, size–abundance spectra of entire plankton ecosystems that span across trophic levels have slopes close to -1 (ref. 24), indicating the loss of available energy with increasing body size in systems where small organisms are generally consumed by larger organisms<sup>25</sup>.

The external (abiotic) control of assemblage structure was evident when population abundances of the three phytoplankton classes were examined in relation to the degree of mixing of the water column (Fig. 3a). Picoplankton were clearly favoured under conditions of high stratification, generally marked by low nutrients and high temperature. As stratification diminished, the balance shifted away from picoplankton and towards large nanoplankton. Under well-mixed conditions, no clear pattern emerged from the sparse data. Throughout the range of mixing conditions, the abundance of small nanoplankton was invariant. Together, these patterns seem to underlie the cytometric diversity (Fig. 3b). At an intermediate level of stratification, a clear maximum in diversity was evident where picoplankton abundance and large nanoplankton abundance converged, from opposing directions, to small nanoplankton abundance (Fig. 3a, b). If it can be agreed that mixing of the water column is a disturbance that has the potential to alter ecological equilibria, then the intermediate disturbance hypothesis<sup>26,27</sup> becomes a useful basis to understand the role of allogenic forcing on processes of marine phytoplankton assembly. Essentially, strong disturbance excludes all but a few robust species whereas weak disturbance allows strong competition; diversity is therefore maximum when the level of disturbance is intermediate. Intermediate disturbance may be viewed as a factor shaping diversity (Fig. 3b) through an equitable distribution of cells in size classes (Fig. 3a), from which arises a high overall biomass (Fig. 2a). This is an idea that easily fits into the current view of how different regimes of turbulence and nutrients influence the prominent life forms of phytoplankton<sup>22</sup>. Somewhere in between the small-cell regime of low turbulence and low nutrients and the large-cell regime of high turbulence and high nutrients lies a regime of high diversity.

Reynolds's thesis that the principles discerned from pelagic microscopic vegetation, subject to scaling adjustments, have general applicability in ecology<sup>27</sup> is a suitable context in which to view the macroecological patterns of phytoplankton. The link now developing between concepts of microbial size spectra, rules of self-organization and hydrodynamic forcing<sup>23,28</sup> is strengthened by the realization that picophytoplankton, small nanophytoplankton and large nanophytoplankton have distinct responses to abiotic control that can shape community structure. □

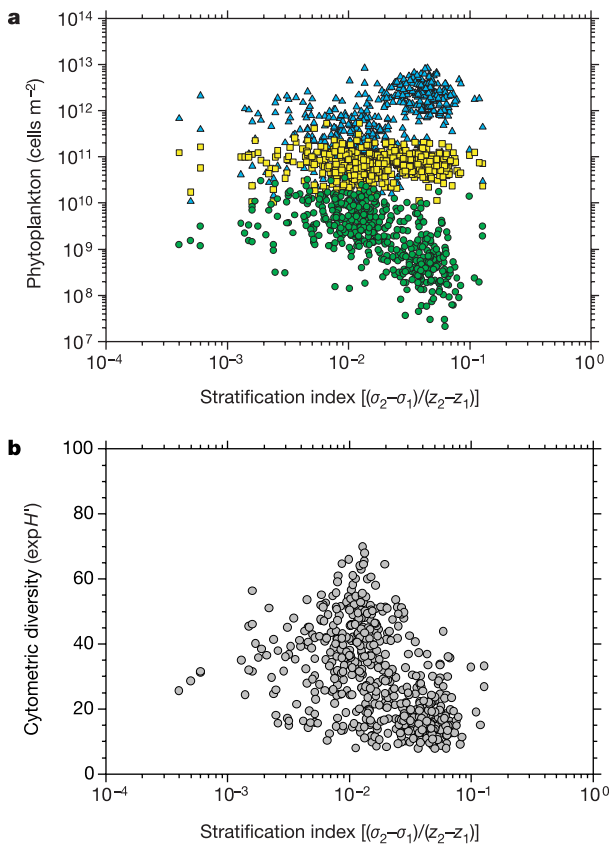


**Figure 3** Influence of water-column stability on phytoplankton abundance (a) and cytometric diversity (b) ( $n = 656$ ). The stratification index is the seawater density ( $\sigma$ ) difference normalized to the depth ( $z$ ) difference, which was about 90 m in most cases. Cytometric diversity was calculated as the abundance-weighted average from 0 to 100 m. Phytoplankton size classes are colour coded as in Fig. 2a.

**Methods**

Chlorophyll *a* was measured in acetone extracts of particulate matter collected on Whatman GFF filters using a Turner Designs fluorometer. Phytoplankton in aliquots

.....  
**Coding of smooth eye movements  
in three-dimensional space  
by frontal cortex**

**Kikuro Fukushima\***, **Takanobu Yamanobe\***, **Yasuhiro Shinmei\***,  
**Junko Fukushima\***, **Sergei Kurkin\*** & **Barry W. Peterson†**

\* *Department of Physiology, Hokkaido University School of Medicine, West 7,  
North 15, Sapporo 060-8638, Japan*

† *Northwestern University Medical School, 303E Chicago Avenue, Chicago,  
Illinois 60611, USA*

.....  
**Through the development of a high-acuity fovea, primates with  
frontal eyes have acquired the ability to use binocular eye move-  
ments to track small objects moving in space<sup>1</sup>. The smooth-  
pursuit system moves both eyes in the same direction to track  
movement in the frontal plane (frontal pursuit), whereas the  
vergence system moves left and right eyes in opposite directions  
to track targets moving towards or away from the observer  
(vergence tracking). In the cerebral cortex and brainstem, signals  
related to vergence eye movements—and the retinal disparity and  
blur signals that elicit them—are coded independently of signals  
related to frontal pursuit<sup>2–6</sup>. Here we show that these types of  
signal are represented in a completely different way in the  
smooth-pursuit region of the frontal eye fields<sup>7–11</sup>. Neurons of  
the frontal eye field modulate strongly during both frontal pur-  
suit and vergence tracking, which results in three-dimensional  
cartesian representations of eye movements. We propose that the  
brain creates this distinctly different intermediate representation  
to allow these neurons to function as part of a system that enables  
primates to track and manipulate objects moving in three-  
dimensional space.**

In two monkeys, we recorded the activity of 225 neurons that was modulated during frontal pursuit and/or vergence tracking of laser spots projected onto a vertical or horizontal screen (Methods). Of 122 neurons tested during both frontal pursuit and vergence tracking, 80 (66%) responded to both (three-dimensional (3D) tracking). Thirty (25%) responded only during frontal pursuit and 12 (9%) responded only during vergence tracking.

Of the 92 neurons that responded during vergence tracking, 39 were activated during divergence (Fig. 1a), 45 during convergence (Fig. 3a, f) and 8 during both (data not shown). The neuron shown in Fig. 1a–d was activated strongly as the monkey tracked a target moving away from him (Fig. 1a) and more weakly during downward pursuit (Fig. 1d). Because the horizontal screen used to present targets moving in depth was at nose level, divergence eye movements were accompanied by small (0.8°) upward eye movements. This combined motion that was required during vergence tracking could not explain the increased discharge of this neuron during divergence, because it was activated during downward pursuit.

Similar arguments could be applied to the 36 neurons that had no response to vertical pursuit, or a response in the wrong direction, to account for their observed modulation during vergence tracking. For neurons whose vertical pursuit sensitivity was in the correct direction to contribute to their modulation during vergence tracking, the contribution was too small to account for the modulation observed during vergence tracking. Figure 2a shows this for a divergence plus upward pursuit neuron whose eye velocity sensitivity at 0.3, 0.5 and 1.0 Hz was much smaller during frontal pursuit than during vergence tracking.

Figure 2b plots the relationship between vergence-tracking and frontal-pursuit (combined horizontal, vertical) sensitivities for five groups of neurons. Sensitivities varied widely with a tendency for

(≤0.5 ml) of sea water were analysed by flow cytometry<sup>29</sup> using a Becton Dickinson FACSort. As population abundance is inversely related to cell size, detection of phytoplankton in the small aliquots was usually limited to cells that were abundant, namely the picophytoplankton (<2 μm) and nanophytoplankton (2–20 μm). The microphytoplankton (>20 μm) were not included in our measurements. This limitation is discussed elsewhere<sup>30</sup>. Although the microphytoplankton contribute significantly to total photoautotrophic biomass at various times and places, they were seldom significant on a numerical basis. Cytometric forward light scatter was calibrated using synthetic microspheres<sup>29</sup> and therefore cannot be assumed to measure accurately the size of phytoplankton cells<sup>28</sup>. However, the approximate positions of 2 μm and 10 μm on the light scatter scale were confirmed by flow cytometric analysis of the phytoplankton assemblage after physical size fractionation using Nuclepore polycarbonate membranes.

Received 23 May; accepted 11 July 2002; doi:10.1038/nature00994.

1. Longhurst, A. *Ecological Geography of the Sea* (Academic, San Diego, 1998).
2. Cole, J., Lovett, G. & Findlay S. (eds) *Comparative Analyses of Ecosystems: Patterns, Mechanisms, and Theories* (Springer, New York, 1991).
3. Gasol, J. M. & Duarte, C. M. Comparative analyses in aquatic microbial ecology: how far do they go? *FEMS Microb. Ecol.* **31**, 99–106 (2000).
4. Li, W. K. W. Annual average abundance of heterotrophic bacteria and *Synechococcus* in surface ocean waters. *Limnol. Oceanogr.* **42**, 1746–1753 (1998).
5. Brown, J. H. *Macroecology* (Univ. Chicago Press, Chicago, 1995).
6. Peters, R. H. *The Ecological Implications of Body Size* (Cambridge Univ. Press, Cambridge, 1983).
7. Brown, J. H. & West, G. B. (eds) *Scaling in Biology* (Oxford Univ. Press, New York, 2000).
8. Li, W. K. W. Cytometric diversity in marine ultraphytoplankton. *Limnol. Oceanogr.* **42**, 874–880 (1997).
9. Sommer, U., Padisák, J., Reynolds, C. S. & Juhász-Nagy, P. Hutchinson's heritage: the diversity-disturbance relationship in phytoplankton. *Hydrobiologia* **249**, 1–7 (1993).
10. Li, W. K. W. & Harrison, W. G. Chlorophyll, bacteria and picophytoplankton in ecological provinces of the North Atlantic. *Deep-Sea Res. II* **48**, 2271–2293 (2001).
11. Chisholm, S. W. in *Primary Productivity and Biogeochemical Cycles in the Sea* (eds Falkowski, P. G. & Woodhead, A. D.) 213–237 (Plenum, New York, 1992).
12. Hill, M. O. Diversity and evenness: a unifying notation and its consequences. *Ecology* **54**, 427–432 (1973).
13. Legendre, P. & Legendre, L. *Numerical Ecology*, 2nd edn (Elsevier, Amsterdam, 1998).
14. Yentsch, C. S. & Phinney, D. A. A bridge between ocean optics and microbial ecology. *Limnol. Oceanogr.* **34**, 1694–1705 (1989).
15. Ciotti, Á. M., Lewis, M. R. & Cullen, J. J. Assessment of the relationships between dominant cell size in natural phytoplankton communities and the spectral shape of the absorption coefficient. *Limnol. Oceanogr.* **47**, 404–417 (2002).
16. Damuth, J. D. Common rules for animals and plants. *Nature* **395**, 115–116 (1998).
17. Enquist, B. J., Brown, J. H. & West, G. B. Allometric scaling of plant energetics and population density. *Nature* **395**, 163–165 (1998).
18. Laws, E. A. & Archie, J. W. Appropriate use of regression analysis in marine biology. *Mar. Biol.* **65**, 13–16 (1981).
19. Montagnes, D. J. S., Berges, J. A., Harrison, P. J. & Taylor, F. J. R. Estimating carbon, nitrogen, protein, and chlorophyll *a* from volume in marine phytoplankton. *Limnol. Oceanogr.* **39**, 1044–1060 (1994).
20. Agustí, S. & Kalfi, J. The influence of growth conditions on the size dependence of maximal algal density and biomass. *Limnol. Oceanogr.* **34**, 1104–1108 (1989).
21. Belgrano, A., Allen, A. P., Enquist, B. J. & Gillooly, J. F. Allometric scaling of maximum population density: a common rule for marine phytoplankton and terrestrial plants. *Ecol. Lett.* (in the press).
22. Cullen, J. J., Franks, P. J. S., Karl, D. M. & Longhurst, A. in *Biological-Physical Interactions in the Sea* (eds Robinson, A. R., McCarthy, J. J. & Rothschild, B. J.) *The Sea Vol. 12* 297–336 (Wiley, New York, 2002).
23. Rodríguez, J. *et al.* Mesoscale vertical motion and the size structure of phytoplankton in the ocean. *Nature* **410**, 360–363 (2001).
24. Rodríguez, J. Some comments on the size-based structural analysis of the pelagic ecosystem. *Sci. Mar.* **58**, 1–10 (1994).
25. Cyr, H. in *Scaling in Biology* (eds Brown, J. H. & West, G. B.) 267–295 (Oxford Univ. Press, New York, 2000).
26. Connell, J. Diversity in tropical rain forests and coral reefs. *Science* **199**, 1304–1310 (1978).
27. Reynolds, C. S. *Vegetation Processes in the Pelagic: a Model for Ecosystem Theory* (Ecology Institute, Oldendorf/Luhe, 1997).
28. Cavender-Bares, K. K., Rinaldo, A. & Chisholm, S. W. Microbial size spectra from natural and nutrient enriched ecosystems. *Limnol. Oceanogr.* **46**, 778–789 (2001).
29. Li, W. K. W. Composition of ultraphytoplankton in the central North Atlantic. *Mar. Ecol. Prog. Ser.* **122**, 1–8 (1995).
30. Li, W. K. W. & Dickie, P. M. Monitoring phytoplankton, bacterioplankton, and viroplankton in a coastal inlet (Bedford Basin) by flow cytometry. *Cytometry* **44**, 236–246 (2001).

**Acknowledgements**

I thank all seagoing staff of the Biological Oceanography Section at Bedford Institute of Oceanography for collecting samples. I am grateful to C. Reynolds, G. Harrison, T. Platt and P. Falkowski for reading the manuscript. I also thank A. Belgrano for sharing his knowledge and pre-publication work on allometry with me. Financial support was provided by DFO Strategic Science Fund in the Ocean Climate Program, and the Interdepartmental Panel on Energy R&D.

**Competing interests statement**

The author declares that he has no competing financial interests.

Correspondence and requests for materials should be addressed to W.K.W.L. (e-mail: Lib@mar.dfo-mpo.gc.ca).

Type of mouse embryonic fibroblast cells	Early passage	Late passage	With activated RAS oncogene	With activated RAS and SV40 T antigen
Wild type	Growth	Senescence	Senescence	Transformation
No <i>p53</i> or <i>Ink4a/ARF</i> tumour suppressors	Growth	Growth	Transformation	Transformation
No <i>Rb</i> and <i>p107</i> ; no <i>Rb</i> , <i>p107</i> and <i>p130</i>	Growth	Growth	Senescence	Transformation
No <i>Lkb1</i>	Growth	Growth	Senescence	No transformation

**Figure 2 A different type of tumour suppressor? The features of the mouse *Lkb1* gene are rather unusual, as seen here. *Rb*, *p107* and *p130* are tumour-suppressor genes of the *Rb* family. SV40 is simian virus 40. Senescence prevents indefinite cell growth (immortalization); transformation refers to processes by which cells become cancer cells. 'Early' and 'late' passage refers to the relative amount of time cells have spent in culture.**

stimuli, such as DNA damage, the expression of activated oncogenes (which promote cell growth), and stress induced by the tissue-culture process<sup>8</sup>.

Bardeesy *et al.* found that their homozygous MEFs were resistant to tissue-culture-induced senescence, and thereby became immortal, but still underwent senescence induced by DNA damage or oncogenes. This suggests that a lack of *Lkb1* renders cells immortal by inhibiting or alleviating the culture-stress-induced activation of senescence. Importantly, however, these immortal MEFs also turned out to be resistant to transformation induced by potent combinations of oncogenes, such as activated *RAS* and SV40 large T antigen, which readily transform normal cells (Fig. 2). So, although the lack of *Lkb1* causes immortalization, the immortalized cells seem to be resistant to subsequent transformation.

So *Lkb1* deficiency is a double-edged sword, somehow promoting perpetual cell growth but preventing malignant transformation — and explaining why the polyps in PJS patients develop yet remain benign. But how does *Lkb1* loss in the intestinal epithelium promote the development of stromal-rich polyps? Bardeesy *et al.* examined the genes expressed in the homozygous MEFs and in polyps from heterozygous mice, and detected marked increases in the expression of various genes encoding components of the extracellular matrix and secreted signalling molecules. So perhaps factors such as these, produced by *Lkb1*-deficient epithelial cells, influence the stromal cells in PJS polyps. In keeping with this idea, the authors observed that homozygous MEFs, and the medium in which these cells were cultured, affected the expression of specific genes in normal MEFs.

An unanswered question is why PJS patients are more likely than usual to develop other types of cancer. This seems odd, given that a lack of *LKB1* prevents malignant transformation of intestinal polyps. Does this mean that *LKB1*-deficient cells are resistant

to transformation by some activated oncogenes (such as members of the *RAS* pathway), but more susceptible to others? The low frequency of activating *RAS* mutations in tumours from PJS patients certainly hints

Ecology

# Oceans under the microscope

Andrea Belgrano and James H. Brown

Phytoplankton are marine algae that support all ocean life, so it is important to understand the processes that control their distribution, abundance and diversity. Macroecology offers a way to do so.

Increasingly, scientists are turning to the relatively new approach of macroecology to study the structure and dynamics of complex ecosystems. Macroecologists look for statistical patterns in the abundance, distribution, biomass and diversity of individual organisms or species, in an effort to understand why these patterns emerge and what processes govern the structure and dynamics of the ecosystem as a whole. At first, macroecology relied heavily on large data sets of quite well-studied terrestrial birds and mammals<sup>1,2</sup>. More recently, the approach and principles have been applied more widely — to fish, plants, molluscs and insects. Now, on page 154 of this issue, Li<sup>3</sup> takes a macroecological approach to biological oceanography.

One problem in understanding the ecology of the oceans is the enormous spatial and temporal variation that results largely from climatic and physical oceanographic fluctuations (see, for example, Fig. 1). How can this problem be overcome so as to discover general features that are due to fundamental organizing processes? This is where the macroecological approach of looking at the statistical patterns of ecosystem components is so useful. For instance, to understand the structure and function of marine ecosystems, it is crucial to determine which

at this possibility. Alternatively, the order of events may matter. For example, *LKB1* inactivation in normal intestinal epithelium might protect those cells from malignant transformation, resulting in benign polyps. But in cell types that have already acquired mutations in other cancer genes, *LKB1* loss might promote tumour progression. No doubt Bardeesy and colleagues' mouse model will prove valuable in addressing these and other issues.

Louise van der Weyden, Jos Jonkers and Allan Bradley are at the Wellcome Trust Sanger Institute, Wellcome Trust Genome Campus, Hinxton CB10 1SA, UK.

e-mail: abradley@sanger.ac.uk

1. Bardeesy, N. *et al.* *Nature* **419**, 162–167 (2002).
2. Haggitt, R. C. & Reid, B. J. *Am. J. Surg. Pathol.* **10**, 871–887 (1986).
3. Kinzler, K. W. & Vogelstein, B. *Science* **280**, 1036–1037 (1998).
4. Wang, Z. J. *et al.* *J. Pathol.* **188**, 613–617 (1999).
5. Ylikorkala, A. *et al.* *Science* **293**, 1323–1326 (2001).
6. Miyoshi, H. *et al.* *Cancer Res.* **62**, 2261–2266 (2002).
7. Jishage, K. *et al.* *Proc. Natl Acad. Sci. USA* **99**, 8903–8908 (2002).
8. Sherr, C. J. *Nature Rev. Mol. Cell Biol.* **2**, 731–737 (2001).

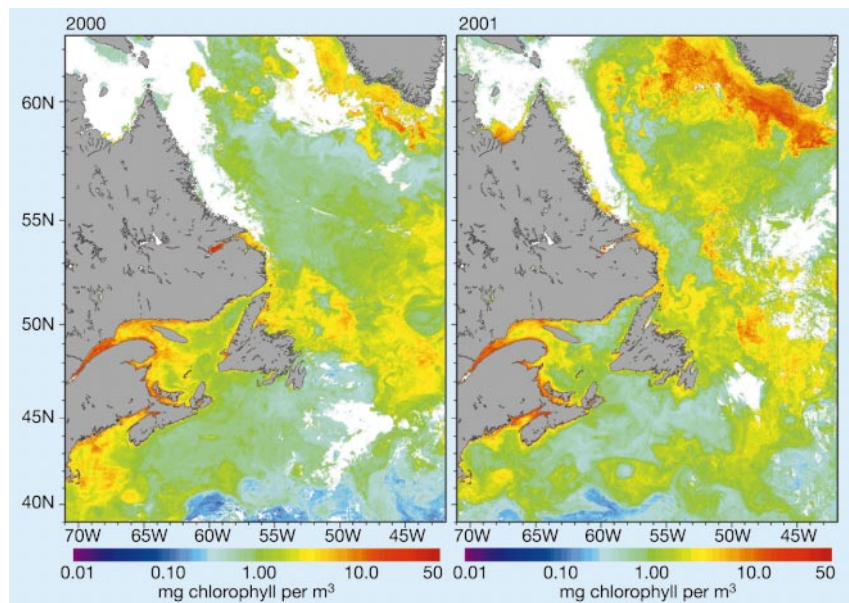


**Figure 1** Biomass of chlorophyll from phytoplankton in surface waters of the northwest North Atlantic Ocean, the area investigated by Li<sup>3</sup>, in two-week periods in 2000 and 2001. The amount of chlorophyll is revealed by images produced from SeaWiFS data, collected by the OrbView-2 satellite, resolved to about 1.5 km per pixel. The images show broad similarities in chlorophyll concentration, as well as some significant differences, from year to year. They also show significant spatial heterogeneity. Li<sup>3</sup> has used macroecological principles to try to disentangle such broad patterns, which probably result from large-scale climatic and physical oceanographic events, from the organizing processes inherent to marine phytoplankton. (These images are composites for 16 May to 30 May in 2000 and 2001, and are available at <http://oceanimage.mar.dfo-mpo.gc.ca>)

This extends to marine phytoplankton the 'energy equivalence rule' that has been demonstrated previously for other groups of organisms, including terrestrial animals and plants<sup>4,5</sup>, suggesting that this rule is very general, if not universal. If all the individuals in a given size class do indeed use energy at the same rate as all the individuals that make up other size classes, this is an important feature of ecological organization that begs a mechanism. So far, it is not clear why organisms from different size classes should have access to, or be able to appropriate, equal quantities of energy.

Li's second important finding is that phytoplankton are most diverse at intermediate levels of chlorophyll concentration, and when the layers of the ocean water column are mixed to a degree somewhere between 'no mixing' and 'complete mixing'. Li obtained this result by measuring phytoplankton diversity not by tallying the number of species — as is traditional in ecology — but by creatively using flow cytometry to quantify the variety of phytoplankton types on the basis of their light-scattering properties. The results suggest that maximal diversity occurs when some intermediate degree of water mixing allows diverse functional types to coexist. (A high degree of mixing would allow one or a few species that can cope well with such disturbance to become dominant; likewise, no disturbance at all would foster competition, again allowing one or a few

superior competitors to become dominant.)

More generally, Li's work<sup>3</sup> shows that, despite the enormous complexity and variety of marine phytoplankton, there are emergent

#### Earth science

## Baked Alaska

Peter Clift and Karen Bice

The warming of the Earth's climate more than 50 million years ago is as yet unexplained. Now the finger points to the heating of sediment in the Gulf of Alaska as an important source of the greenhouse gas methane.

Between about 58 and 52 million years ago, during the late Palaeocene and early Eocene epochs, the Earth's climate warmed considerably. What was the cause of this unusually long warming trend? Writing in *Geology*, Hudson and Magoon<sup>1</sup> put forward an idea that adds to thinking on the subject.

The marine geological record shows that Earth's climate has experienced swings of cooling and heating over various timescales. Change over thousands to hundreds of thousands of years seems to be related to orbital variations, but climate trends lasting millions of years have been harder to explain. The interval between the late Palaeocene and early Eocene has attracted particular interest, not only because of the exceptional

features of phytoplankton abundance and diversity that are related to cell size and overall chlorophyll content, respectively. The implication is that it is possible to make mechanistic connections between the metabolism of individual organisms (in this case, phytoplankton) and the roles of those organisms in ecosystems (here, in the productivity and feeding dynamics of oceans). For example, a recent study<sup>6</sup> of marine food webs suggests how oceanographic and climatic events, through their effects on the abundance and productivity of phytoplankton, can cause fluctuations in commercial fish stocks.

Ecology has generally lacked unifying theories. Much of the emphasis has been on the seemingly large differences between different kinds of organisms and ecosystems, and on the extensive spatial and temporal variation within ecosystems. Now, however, there is increasing evidence that some macroecological patterns and mechanistic processes hold across diverse taxa and ecological systems. Such generality suggests exciting prospects for conceptual unification. ■

Andrea Belgrano and James H. Brown are in the Department of Biology, University of New Mexico, 167 Castetter Hall, Albuquerque, New Mexico 87131-1091, USA.  
e-mail: [belgrano@unm.edu](mailto:belgrano@unm.edu)

1. Brown, J. H. *Macroecology* (Chicago Univ. Press, 1995).
2. Gaston, K. J. & Blackburn, T. M. *Pattern and Process in Macroecology* (Blackwell, Oxford, 2000).
3. Li, W. K. W. *Nature* **419**, 154–157 (2002).
4. Damuth, J. *Nature* **290**, 699–700 (1981).
5. Enquist, B. J., Brown, J. H. & West G. B. *Nature* **395**, 163–165 (1999).
6. Stenseth, N. C. *et al. Science* **297**, 1292–1296 (2002).